

- R. Heumann, *J. Cell Biol.* **121**, 665 (1993).
9. L. C. Cantley *et al.*, *Cell* **64**, 281 (1991).
  10. P. T. Hawkins, T. R. Jackson, L. R. Stephens, *Nature* **358**, 157 (1992).
  11. A. N. Carter and C. P. Downes, *J. Biol. Chem.* **267**, 14563 (1992); M. Ohmichi, S. J. Decker, A. R. Saltiel, *Neuron* **9**, 769 (1992); S. P. Soltoff, S. L. Rabin, L. C. Cantley, D. R. Kaplan, *J. Biol. Chem.* **267**, 17472 (1992); S. Raffioni and R. A. Bradshaw, *Proc. Natl. Acad. Sci. U.S.A.* **89**, 9121 (1992).
  12. P. Rodriguez-Viciana *et al.*, *Nature* **370**, 527 (1994).
  13. H. Yano *et al.*, *J. Biol. Chem.* **268**, 25846 (1993); T. Okada, Y. Kawano, T. Sakakibara, O. Hazeki, M. Ui, *ibid.* **269**, 3568 (1994); T. Okada, L. Sakuma, Y. Fukui, O. Hazeki, M. Ui, *ibid.*, p. 3563.
  14. K. Kimura *et al.*, *J. Biol. Chem.* **269**, 18961 (1994).
  15. Y. Gavrieli, Y. Sherman, S. A. Ben-Sasson, *J. Cell Biol.* **119**, 493 (1992); L. L. Kelley *et al.*, *Mol. Cell Biol.* **14**, 4183 (1994).
  16. L. Stephens *et al.*, *Cell* **77**, 83 (1994).
  17. C. J. Vlahos, W. F. Matter, K. Y. Hui, R. F. Brown, *J. Biol. Chem.* **269**, 5241 (1994).
  18. PC-12 cells expressing wild-type or Y740F mutant receptors were isolated and characterized by R. R. Vaillancourt and G. L. Johnson (National Jewish Center for Immunology and Respiratory Medicine, Denver, CO). Human PDGF  $\beta$  receptors were introduced into PC-12 cells by means of the pLXSN retrovirus vector. Cells were maintained in Dulbecco's modified Eagle's medium (DMEM) supplemented with 5% plasma-derived horse serum and 5% plasma-derived newborn calf serum (Cocalico Biologicals, Reamstown, PA) in dishes coated with poly-L-lysine.
  19. A. Kashishian, A. Kazlauskas, J. A. Cooper, *EMBO J.* **11**, 1373 (1992); A. Kazlauskas, A. Kashishian, J. A. Cooper, M. Valius, *Mol. Cell Biol.* **12**, 2534 (1992).
  20. R. Nishimura *et al.*, *Mol. Cell Biol.* **13**, 6889 (1993).
  21. L. E. Heasley and G. L. Johnson, *Mol. Biol. Cell* **3**, 545 (1992).
  22. A. Obermeier *et al.*, *EMBO J.* **13**, 1585 (1994).
  23. H. Nakanishi, K. A. Brewer, J. H. Exton, *J. Biol. Chem.* **268**, 13 (1993).
  24. J. K. Chung, T. C. Grammer, K. P. Lemon, A. Kazlauskas, J. Blenis, *Nature* **370**, 71 (1994).
  25. S. Roche, M. Koegl, S. A. Courtneidge, *Proc. Natl. Acad. Sci. U.S.A.* **91**, 9185 (1994); B. H. Jhun *et al.*, *Mol. Cell Biol.* **14**, 7466 (1994); B. Cheatham *et al.*, *ibid.*, p. 4902; K. Hara *et al.*, *Proc. Natl. Acad. Sci. U.S.A.* **91**, 7415 (1994); M. Joly, A. Kazlauskas, F. S. Fay, S. Corvera, *Science* **263**, 684 (1994); K. Kotani *et al.*, *EMBO J.* **13**, 2313 (1994).
  26. R. Yao and G. M. Cooper, unpublished results.
  27. Y. Gotoh *et al.*, *Eur. J. Biochem.* **193**, 661 (1990).
  28. D. Hockenbery, G. Nuñez, C. Millman, R. D. Schreiber, S. J. Korsmeyer, *Nature* **348**, 334 (1990).
  29. We thank R. R. Vaillancourt and G. L. Johnson for PC-12 cells expressing PDGF receptors. This research was supported by NIH grant RO1 CA 18689.

12 September 1994; accepted 13 February 1995

## High-Frequency Motility of Outer Hair Cells and the Cochlear Amplifier

Peter Dallos\* and Burt N. Evans

Outer hair cells undergo somatic elongation-contraction cycles *in vitro* when electrically stimulated. This "electromotile" response is assumed to underlie the high sensitivity and frequency selectivity of amplification in the mammalian cochlea. This process, presumably operating on a cycle-by-cycle basis at the frequency of the stimulus, is believed to provide mechanical feedback *in vivo*. However, if driven by the receptor potential of the cell, the mechanical feedback is expected to be severely attenuated at high frequencies because of electrical low-pass filtering by the outer hair cell basolateral membrane. It is proposed that electromotility at high frequencies is driven instead by extracellular potential gradients across the hair cell, and it is shown that this driving voltage is not subject to low-pass filtering and is sufficiently large. It is further shown that if the filtering properties of the cell membrane are canceled, taking advantage of the electrical characteristics of isolated outer hair cells in a partitioning glass microchamber, then the lower bound of the motor's bandwidth is approximately 22 kilohertz, a number determined only by the limitations of our instrumentation.

It is a common assumption that mammalian hearing owes its remarkable sensitivity and frequency-resolving capabilities to a local mechanical feedback process within the cochlea [for review, see (1)]. This process has been termed the "cochlear amplifier" (2) and it is assumed that its motor arm is a somatic shape change of outer hair cells (OHCs) (3). Such shape changes can be elicited by a natural stimulus to the cell [that is, stereociliary deflection (4)] and therefore can be driven *in vivo*. In order to be an effective form of mechanical feedback, somatic length changes are thought to occur on a cycle-by-cycle basis, counteracting the mechanical damping of the cochlear partition. Inasmuch as the high-frequency boundary of mammalian hearing exceeds 20 kHz in most species and 100 kHz in some, somatic length changes need to be made at

remarkable speeds. It is known that distortion product otoacoustic emissions, assumed to be related to OHC motility in mammals, occur up to at least 100 kHz (5).

Because the receptor potential is severely attenuated at high frequencies due to the resistance-capacitance (RC) filtering of the cell membrane (6), it is difficult to understand how it may drive the cell's own motility except at relatively low frequencies in the apex of the cochlea, where OHC receptor potentials are sufficient to produce large electromotile responses. It is estimated that OHC motility in the 16- to 18-kHz range, where measurements are available, is about 20% of basilar membrane motion (7). It thus appears that the generally accepted model of cochlear amplification becomes questionable as the intracellular response becomes too small to drive motility at high frequencies where OHC motility presumably occurs in many small mammals. We propose that the effective electrical stimulus that powers the OHC motile response at high frequencies is not the cell's own recep-

tor potential, but an extracellular voltage gradient, established across the hair cell, between the scala media and intra-organ of Corti fluid spaces. These gross potentials reflect voltage drops on the bulk impedance of the organ of Corti that are due to the weighted vector sum of receptor currents produced by all sound-stimulated OHCs.

For consideration of such a proposition, three questions need to be examined. First, why would not these extracellular voltages be subject to filtering limitations similar to those on the intracellular receptor potential? Second, is the extracellular potential larger than the intracellular one at high frequencies? Third, are the OHC motors intrinsically capable of responding in the high kilohertz range? The last issue has its own biological significance, because in order to understand the nature of the aggregate of molecular motors (3, 8) that powers motility, it is of interest to determine its inherent speed. At this time, due to experimental limitations, quantitative data on the speed of motility have been reported only up to approximately 1 kHz (6).

Outer hair cells are partitioned *in vivo* between two fluid compartments: endolymph of the scala media and perilymph within the organ of Corti (Fig. 1A). OHCs dominate the production of extracellular stimulus-related potentials, which are voltage drops due to the receptor current on the various bulk impedances of cochlear tissues. Although the electrical circuit of the cochlea is complex, one can estimate (9) that, owing to the small shunt resistance, the total impedance between scala media and organ of Corti fluid space has a flat magnitude between ~6 and ~300 kHz. It is also known that extracellular ac electrical responses can be measured up to at least 100 kHz (10). Thus, extracellular voltage gradients are not significantly filtered.

The microchamber technique (11) simulates the electrical partitioning that exists in epithelia, such as the organ of Corti (Fig.

Auditory Physiology Laboratory (The Hugh Knowles Center), Departments of Neurobiology and Physiology and Communication Sciences and Disorders, Northwestern University, Evanston, Illinois 60208, USA.

\*To whom correspondence should be addressed.

1B), and makes it possible to measure the dynamic properties of the putative motors themselves. We show that such partitioning of the OHC, whether in vivo (Fig. 1A) or in vitro in the microchamber (Fig. 1B), produces electrical conditions with extrinsic electrical stimuli that result in motile behavior as if the electrical filter properties of the cell membrane were canceled. When the cell is so partitioned, it is possible to drive OHC motility either by imposing voltage gradients across the cochlear partition in an experimental situation (12) or, as proposed here, by the extracellular receptor potential in vivo.

To derive the frequency response behavior of a partitioned OHC, either in situ or when inserted into the microchamber, the electrical impedances of the two cell membrane segments facing endolymph (apical) and perilymph (basolateral), respectively (or those outside and inside the microchamber), are represented as  $Z_a$  and  $Z_b$ . These impedances are derived from the parallel resistance ( $R$ ) and capacitance ( $C$ ) of the membrane, with  $\tau = RC$  and  $\omega = 2\pi f$ , where  $f$  is the frequency and  $j = \sqrt{-1}$ :

$$Z_a = \frac{R_a}{1 + j\omega\tau_a}; \quad Z_b = \frac{R_b}{1 + j\omega\tau_b} \quad (1)$$

The voltage drop ( $\delta V$ ) on the motor-bearing basolateral membrane segment (included in the microchamber) due to a command voltage,  $V_c$ , across the cochlear partition (microchamber) is (Fig. 1):

$$\delta V = V_c \frac{Z_b}{Z_a + Z_b} \quad (2)$$

Electromotility is driven by the voltage drop,  $\delta V$ , across the motors in the basolateral membrane. This  $\delta V$  is obtained by substitution of Eq. 1 into Eq. 2:

$$\delta V = V_c \frac{R_b}{R_a + R_b} \frac{1 + j\omega\tau_a}{1 + j\omega \frac{R_a\tau_b + R_b\tau_a}{R_a + R_b}} \quad (3)$$

The magnitude of this voltage changes from  $V_c R_b / (R_a + R_b) = V_c \alpha / (1 + \alpha)$ , determined by a resistive voltage divider, at low frequencies ( $\omega \rightarrow 0$ ), to  $V_c R_b \tau_a / (R_b \tau_a + R_a \tau_b) = V_c C_a / (C_a + C_b) = V_c \zeta / (1 + \zeta)$ , determined by a capacitive voltage divider, at very high frequencies ( $\omega \rightarrow \infty$ ). The  $R_b/R_a$

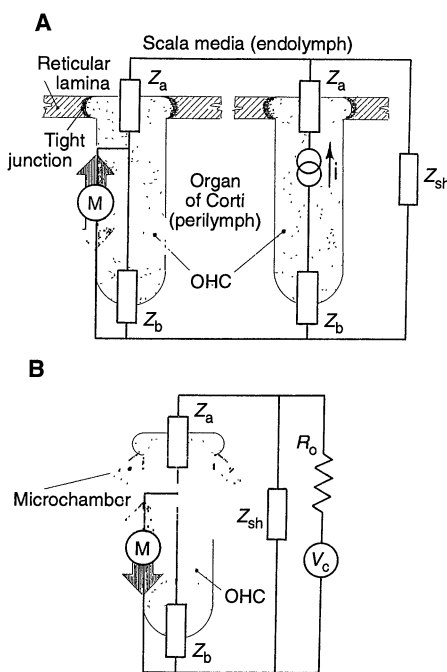
$= \alpha$  and  $C_a/C_b = \zeta$  substitutions are used. The key conclusion is that even at high frequencies, the voltage drop on the cell's basolateral membrane is finite; it is simply changed from its low-frequency value by the factor:

$$\frac{\zeta(1 + \alpha)}{\alpha(1 + \zeta)} \quad (4)$$

Phase shift, determined from Eq. 3, is zero at both  $\omega \rightarrow 0$  and  $\omega \rightarrow \infty$  and is less than  $\pm\pi/2$  in the midfrequency transition region. In other words, for voltages impressed across the cell, either by the extracellular receptor potential gradient in vivo or the command voltage in the microchamber, the voltage drop on the basolateral membrane has finite magnitude and zero phase shift at both low and high frequencies, with a transition region at some middle frequency. Depending on the relative magnitudes of  $\alpha$  and  $\zeta$ , the high-frequency asymptote may be smaller or larger than the low-frequency one, and the mid-frequency phase may be lag or lead. Thus, the electrical configuration represents a quasi-all-pass system. This answers the first question posed above. All-pass filtering is understood when one considers that the voltage applied to the motors in the basolateral membrane develops across the RC filter of that membrane. At the same time, the RC filter of the apical cell membrane is electrically in series with that of the basolateral cell membrane. If the time constants of the two filters are the same, then their filtering effects cancel and a flat all-pass filter is obtained. If  $\tau_1 \neq \tau_2$  and if voltage-dependent conductances and capacitances (13-15) alter the time constants and influence the frequency response, it can still be described as quasi-all-pass, in that aside from mid-frequency gain and phase changes, all frequencies produce responses. Both the zero- and infinite-frequency asymptotes of the frequency response functions have zero slopes (Fig. 2, smooth line). The description applies to hair cells in vivo or in the microchamber for constant voltage command. The consequences are that, first, extracellular receptor potentials could theoretically drive OHC motility even at very high frequencies; and second, the microchamber configuration provides a suitable electrical circuit in which the speed of the motors themselves can be measured (see below).

The experimentally obtained pattern changes from a low-frequency asymptote below 200 Hz to a high-frequency asymptote above 2 kHz. It is seen that the high-frequency asymptote of the magnitude pattern has zero slope. This means that beyond the midfrequency decline, up to the limit of measurement, 22.5 kHz, the magnitude response of the motors is undiminished. The separation between low-

**Fig. 1. (A)** Schematic illustration of OHCs in the epithelium of the organ of Corti. The cells are sealed into the roof of the organ of Corti, the reticular lamina, by tight junctions. The endolymph-facing cellular apex has an electrical impedance of  $Z_a$ , whereas the perilymph-facing basolateral membrane impedance is  $Z_b$ . The motility motor is symbolized by  $M$ , with arrows indicating principal displacement direction. One cell is arbitrarily shown as a current source ( $i$ ), the other as a feedback motor element. All cells within the acoustically excited segment of the organ of Corti are assumed to be both current sources and motor elements. Shunt impedance between scala media and organ of Corti fluid is denoted by  $Z_{sh}$ . The OHC transducer current is produced in vivo by the modulation of  $Z_a$  by means of mechanically activated transducer conductance (23). This modifies a standing current maintained by the biological batteries embodied in the positive polarization of the endolymph and in the hair cell's negative resting potential. For simplicity, we show only a current source. **(B)** Schematic illustration of an OHC fully inserted into the microchamber. A simplified circuit is superimposed to show current path due to external command voltage,  $V_c$ . Membrane impedances of excluded and included segments are  $Z_a$  and  $Z_b$ . Displacement of the included pole is measured; it is driven by the aggregate of motors, symbolized by  $M$ . The microchamber itself may be modeled as a series resistance ( $R_o$ ) and a shunt impedance ( $Z_{sh}$ ), which is in parallel with the hair cell's total series impedance ( $Z_{hc} = Z_a + Z_b$ ). The cell in the microchamber is in the same electrical configuration as in situ (Fig. 1A). At any frequency, the hair cell presents an RC load to the microchamber. The values of  $R_{sh}$  and  $\tau_{sh}$  may be estimated from electrical measurements of the microchamber;  $R_{sh}$  ranges between 5 and 20 megohm, whereas  $\tau_{sh}$  is between 0.01 and 0.03 ms. The measurement of  $R_o$  from the resistance of the microchamber without the cell ( $\sim 0.5$  megohm) provides an overestimate, inasmuch as the access resistance to the cell is less than the (measured) resistance of the chamber's orifice, because of the different surface areas. Using the values of  $R_o = 0.5$  megohm,  $\tau_{sh} = 0.02$  ms and  $R_{sh} = 5$  megohm and the hair cell parameters  $R_{hc}$  and  $\tau_{hc}$  estimated from Housley and Ashmore (13) for apical (long) cells used by us, we estimated the corner frequency of voltage drop across the hair cell to be above 30 kHz. In consequence, the effect of the microchamber on the voltage delivered to the hair cell is very small in the frequency range used in our experiments ( $<23$  kHz) and may be disregarded.



and high-frequency asymptotes varies with cell length, extrusion from the microchamber, and the condition of the cells. All cells, however, conform to the general pattern of having either flat or minimally sloping high-frequency asymptotes.

The present technique of measuring the speed of motility permits an approximately 20-fold improvement in bandwidth beyond that possible by other means (6). We note that, when the electrical effects of the cell membrane are canceled, the wide bandwidth of the remaining dynamic elements—the putative motors themselves—is revealed. It thus seems reasonable to conclude from our experiments that the aggregate of molecular motors possesses a time constant less than  $\sim 44 \mu\text{s}$ . In answer to our third question, the molecular motors themselves are apparently capable of responding with remarkable speed, orders of magnitude faster than any biological motor studied to date. The putative motor proteins may be unique to cochlear OHCs, where they are likely to be manifested as large particles that cover  $\sim 70\%$  of the cell's surface (16). Neither cochlear inner hair cells, nor cochlear supporting cells, nor any other known cell type sustains the fast voltage-driven somatic displacements discussed here.

The postulated driving voltage at high frequencies for OHC motility in vivo is the gradient of the extracellular receptor potentials measured between the scala media and in the organ of Corti. Toward higher frequencies, the scala media potential becomes less important because of the high shunt capacitance of the scala media space. At the behavioral threshold and at the best frequencies of 16 to 18 kHz, the median response for the three best available recordings from the organ of Corti is  $\sim 110 \mu\text{V}$  (17). This entire voltage gradient, however, cannot be used to drive motility. The fraction of this driving voltage that appears across the OHC's basolateral membrane (across the motors) is obtained at high frequencies from the reactive voltage divider as indicated by Eq. 3. Inasmuch as the voltage divider ratio at high frequencies is determined by the capacitance

of the cell membrane segments  $[C_a/(C_a + C_b)]$ , which in turn are determined by surface areas, one can compute the ratio from cell geometry. An updated value from (18) for a  $20\text{-}\mu\text{m}$  (basal) cell is 0.2, yielding an estimated basolateral membrane voltage of  $\sim 22 \mu\text{V}$ , producing an electromotile displacement of  $\sim 0.11 \text{ nm}$  at the behavioral threshold. At this same level, basilar membrane displacement is approximately  $0.16 \text{ nm}$  (19). Considering the uncertainties in determining extracellular voltages and of extrapolating the gain of electromotility from in vitro measurements to in vivo values, one may conclude that, in answer to our second question, OHC displacements caused by extracellular receptor potentials are probably commensurate with basilar membrane displacement, making the proposed mechanism a reasonable candidate for the cochlear amplifier (20). Whether the numbers are accurate is secondary to the principle: Although the intracellular receptor potential must decrease with frequency due to filtering, the extracellular response remains approximately constant. Thus there is a location in the cochlea where, at the best frequency, the extracellular response becomes dominant. Extrapolation predicts the crossover to occur in the guinea pig at  $\sim 6 \text{ kHz}$ , corresponding to the midpoint along the cochlea.

Passively conducted voltages, attenuated by the core conductor properties of the cochlear fluid spaces, could produce electromotile responses away from the region of maximal traveling wave amplitude. Such responses, however, would not couple to the basilar membrane on the apical side of the best frequency, because the OHC motile frequency is above the basilar membrane's mechanical cutoff frequency. Basally conducted voltages could produce a limited extension of the feedback region. Although electrical signals spread over considerable distances in the outer scalae of the cochlea, the space constant of the organ of Corti fluid compartment is estimated to be less than  $0.3 \text{ mm}$  (21). Consequently, the putative control signal is well localized.

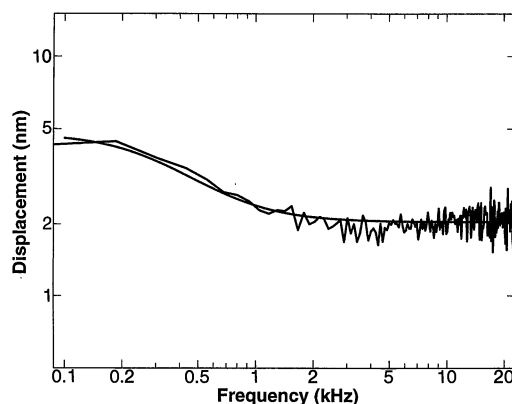
There is no priori reason why the above

scheme could not be operational even at ultrasonic frequencies or be used by other systems. Tuberosus electroreceptors in some mormyrid fish respond to ac electric fields having frequencies above  $10 \text{ kHz}$ . Knollenorgans in *Pollimyrus isidori*, for example, can be tuned to frequencies as high as  $18 \text{ kHz}$  (22). These electroreceptors are incorporated in tight epithelia, not unlike hair cells, and they too should respond to extrinsic fields in a similar quasi-all-pass manner.

## REFERENCES AND NOTES

1. P. Dallos, *J. Neurosci.* **12**, 4575 (1992).
2. H. Davis, *Hearing Res.* **9**, 79 (1983).
3. W. E. Brownell, C. R. Bader, D. Bertrand, Y. de Ribaupierre, *Science* **227**, 194 (1985); B. Kachar, W. E. Brownell, R. A. Altschuler, J. Fex, *Nature* **322**, 365 (1986); H. P. Zenner, *Hearing Res.* **22**, 83 (1986); J. F. Ashmore, *J. Physiol. (London)* **388**, 323 (1987).
4. B. N. Evans and P. Dallos, *Proc. Natl. Acad. Sci. U.S.A.* **90**, 8347 (1993).
5. M. Kössl, *Hearing Res.* **60**, 156 (1992).
6. J. Santos-Sacchi, *J. Neurosci.* **12**, 1906 (1992).
7. At  $1 \text{ kHz}$ , one may estimate the peak amplitude of the receptor potential as  $\sim 0.3 \text{ mV}$  [P. Dallos, *J. Neurosci.* **5**, 1591 (1985)] at the behavioral threshold of the guinea pig [approximately  $10 \text{ dB}$  of sound pressure; R. R. Fay, *Hearing in Vertebrates: A Psychophysical Databook* (Hill-Fay, Winnetka, IL, 1988)]. Use of the in vitro gain of electromotility of  $10 \text{ nm/mV}$  produces OHC motility of  $\sim 3 \text{ nm}$ , which is in excess of estimated low-frequency basilar membrane motion [N. P. Cooper and W. S. Rhode, in *Biophysics of Hair Cell Sensory Systems*, H. Duifhuis, J. W. Horst, P. van Dijk, S. M. van Netten, Eds. (World Scientific, Singapore, 1993), pp. 249–264]. Extrapolation from direct measurements in guinea pig basal-region OHCs to behavioral threshold sound level ( $\sim 6 \text{ dB}$ ) at  $16$  to  $18 \text{ kHz}$  yields a maximum expected OHC response of  $7.2 \mu\text{V}$  [taking the mean plus 2 SD from (17)]. Using a lesser gain of motility of  $5 \text{ nm/mV}$  to account for the fewer motors in shorter OHCs, one estimates a motile response of only  $0.036 \text{ nm}$ . This is less than the corresponding basilar membrane motion of  $\sim 0.16 \text{ nm}$  (19). When the gain of electromotility is estimated, it is considered that low gain figures are measured in cells voltage-clamped to the in vivo resting potential of  $-70 \text{ mV}$  (3, 6). High values are obtained in the microchamber [P. Dallos, R. Hallworth, B. N. Evans, *J. Neurophysiol.* **70**, 299 (1993)]. Both methods suffer from inherent problems. In voltage-clamped cells, the integrity of the cell membrane, and hence that of the cell's mechanical performance, is compromised. In the microchamber, the resting membrane potential is unknown and the cells may be depolarized, producing more linear responses and higher gain. It is reasonable to assume that the gain of motility in vivo is higher than the low estimate and lower than the high. Hence we use a value of  $10 \text{ nm/mV}$  here for long cells ( $60$  to  $75 \mu\text{m}$ ).
8. P. Dallos, B. N. Evans, R. Hallworth, *Nature* **350**, 155 (1991); F. Kalinec, M. C. Holley, K. Iwasa, D. J. Lim, B. Kachar, *Proc. Natl. Acad. Sci. U.S.A.* **89**, 8671 (1992).
9. M. W. Cannon Jr., thesis, Syracuse University, Syracuse, NY (1976).
10. D. E. Crowley and M. C. Hepp-Reymond, *J. Comp. Physiol. Psychol.* **62**, 427 (1966); G. D. Pollak, O. W. Henson Jr., A. Novick, *Science* **176**, 66 (1972).
11. B. N. Evans, P. Dallos, R. Hallworth, in *Cochlear Mechanisms*, J. P. Wilson and D. T. Kemp, Eds. (Plenum, New York, 1989), pp. 205–206; B. N. Evans, R. Hallworth, P. Dallos, *Hearing Res.* **52**, 288 (1991).
12. A. E. Hubbard and D. C. Mountain, *Science* **222**, 510 (1983); A. L. Nuttall and D. F. Dolan, in *Biophysics of Hair Cell Sensory Systems*, H. Duifhuis, J. W. Horst, P. van Dijk, S. M. van Netten, Eds. (World Scientific, Singapore, 1993), pp. 288–295; G. K. Yates and D. L. Kirk, *ibid.*, pp. 352–359; S. Xue, D. C. Mountain, A. E. Hubbard, *ibid.*, pp. 361–368; F. Mammano and J.

**Fig. 2.** Representative example of experimentally obtained (24) and model frequency response functions of OHCs fully inserted in the microchamber. The smooth line represents model calculation from Eq. 3 with the use of the following parameters:  $\alpha = R_b/R_a = 0.15$ ,  $\zeta = C_a/C_b = 0.06$ ,  $\tau_a = 0.23 \text{ ms}$ ,  $\tau_b = 0.58 \text{ ms}$ . These are obtained by first estimating  $\zeta$  from the ratio of apical and basolateral surface areas of the cell. Then  $\alpha$  is computed from Eq. 4, and the time constants are determined by curve fitting.



F. Ashmore, *Nature* **365**, 838 (1993).

13. G. D. Housley and J. F. Ashmore, *J. Physiol. (London)* **448**, 73 (1992).

14. J. F. Ashmore and R. W. Meech, *Nature* **322**, 368 (1986); A. H. Gitter and H. P. Zenner, in *Basic Issues in Hearing*, H. Duifhuis, J. W. Horst, H. P. Wit, Eds. (Academic Press, London, 1988), pp. 32–39; J. F. Ashmore, in *Cochlear Mechanisms*, J. P. Wilson and D. T. Kemp, Eds. (Plenum, New York, 1989), pp. 107–113; J. Santos-Sacchi, *J. Neurosci.* **11**, 3096 (1991).

15. J. Santos-Sacchi and D. P. Dilger, *Hearing Res.* **35**, 143 (1988).

16. A. Forge, *Cell Tissue Res.* **265**, 473 (1991).

17. M. Kössl and I. J. Russell, *J. Neurosci.* **12**, 1575 (1992); I. J. Russell and M. Kössl, *Proc. R. Soc. London B* **247**, 97 (1992). The values used here for extracellular responses were confirmed by I. J. Russell as being representative of the most sensitive preparations.

18. P. Dallos, *Hearing Res.* **12**, 89 (1983).

19. P. M. Sellick, R. Patuzzi, B. M. Johnstone, *J. Acoust. Soc. Am.* **72**, 131 (1982).

20. Control of cochlear amplification by extracellular voltages has been mentioned in passing by a number of authors, for example, H. Davis [*Am. J. Otolaryngol.* **2**, 153 (1981)] and (15).

21. C. D. Geisler, G. K. Yates, R. B. Patuzzi, B. M. Johnstone, *Hearing Res.* **44**, 241 (1990); M. A. Cheatham and P. Dallos, unpublished data.

22. C. D. Hopkins, *Am. Zool.* **21**, 211 (1981).

23. A. J. Hudspeth and D. P. Corey, *Proc. Natl. Acad. Sci. U.S.A.* **74**, 2407 (1977).

24. Detailed descriptions of the experimental methods have been published (17). OHCs were obtained from the cochleas of young anesthetized albino guinea pigs (care and maintenance of animals was in accord with institutional guidelines). For these specific experiments, cells ( $n = 12$ ) were harvested only from the third and fourth turns of the cochlea; their lengths ranged between 60 and 75  $\mu\text{m}$  and their diameter was uniform (8 to 9  $\mu\text{m}$ ). In other experiments, with cells not fully inserted into the microchamber ( $n = 206$ ), the full range of cell lengths was used. We note that the all-pass nature of the response applies to cells of any length and for any degree of insertion. After removal of segments of the organ of Corti, cells were transferred after enzymatic incubation with Type IV collagenase (0.5 mg/ml; Sigma) to the experimental bath containing either Leibovitz's L-15 medium (Gibco) or Medium 199 (Gibco), supplemented with 15 mM HEPES and 5 mM bovine serum albumin (Sigma) and adjusted to 300 mosM (pH 7.35). Microchambers that held the cells were fabricated from borosilicate glass and had aperture diameters similar to those of OHCs. Cells were drawn into siliconized microchambers by gentle suction. Inserted cells were inspected at high magnification and discarded if there was any sign of induced trauma. All experiments were conducted at room temperature. Electrical command signals were generated from the low-impedance output of a waveform generator board in an IBM 486 clone and were delivered between the electrolytes surrounding and filling the microchamber. Making the fluid within the microchamber positive hyperpolarized the included membrane segment and depolarized the excluded membrane (17). Although the microchamber method did not permit us to measure it directly, the asymmetry of the electromotile response is indicative of the cell's resting potential. Cells that are likely to have relatively high resting potentials produce larger shortening than extension-directed responses. Conversely, depolarized cells generate either a symmetrical electromotile response or one with extension dominance (17) [J. Santos-Sacchi, *J. Neurosci.* **9**, 2954 (1989)]. All cells in this study had pronounced contraction-directed response asymmetry and, by inference, high membrane potential. Pseudorandom noise is often used to identify the linear filter portion of a nonlinear physiological system [A. R. Møller, *Scand. J. Rehab. Med. Suppl.* **3**, 37 (1974); P. A. Marmarelis and V. Z. Marmarelis, *Analysis of Physiological Systems* (Plenum, New York, 1978)]. We used this signal in order to reduce data collection time. For our parameters, the 3-dB down point of the input was at 19,924 Hz. There are 161 spectral compo-

nents within this bandwidth, and the voltage applied across the entire cell per spectral line was approximately  $\pm 0.6$  mV. The extensive data obtained with ternary noise was confirmed in several cells by use of sinusoidal stimuli. The noise floor for the measurement shown in Fig. 2 was between 0.1 and 0.2 nm; thus, noise was clearly not a determinant of the high-frequency asymptote. The cell was imaged through a slit on a photodiode. Cell contraction and expansion modulated the light flux and the photocurrent. The entire stimulus-delivery and measuring apparatus was calibrated by use of the ternary signal input to illuminate the photodiode with a wide-band light-emitting diode and by mea-

surement of its output. The resulting frequency response (corner frequency 18 kHz) of the entire system was used to correct all experimental data. System gain was calibrated for each experimental run by controlled displacement of the image of the cell in the slit.

25. We thank our colleagues M. A. Cheatham, B. Clark, S. Echterler, G. Emadi, D. Z. Z. He, M. Ruggero, J. Siegel, I. Sziklai, and S. Vranic-Sowers for their contributions and their comments on the manuscript. Supported by NIH and the American Hearing Research Foundation.

7 September 1994; accepted 27 December 1994

## TECHNICAL COMMENTS

### Models of $\text{Ca}^{2+}$ Release Channel Adaptation

Channel adaptation (1) involves complex behavior of the sarcoplasmic reticulum (SR)  $\text{Ca}^{2+}$  release channel (ryanodine receptor, RyR). The adaptive behavior is different from conventional ion channel behavior in that adapting channels transiently activate (open) in response to repeated increments of agonist ( $\text{Ca}^{2+}$ ). No published kinetic model known to us could adequately account for this adaptation. We propose a model that readily accounts for the complexities associated with adaptation.

The model is based on the established tetrameric RyR channel structure. Biochemical studies indicate that at least three high affinity  $\text{Ca}^{2+}$ -binding sites exist per monomer (2). We postulate that one kind of binding site (the O-domain) tends to open the channel when activated by  $\text{Ca}^{2+}$  and another (the A-domain) tends to close (adapt) it. Thus, the tetramer would then have four O-domains and four A-domains. The model uses the following rules to describe the behavior of the channel. The channel opens when the number of occupied O-domains (O) on the tetramer exceeds or equals the number of active A-domains (A), that is,  $O \geq A$ . However when  $A > O$ , or  $O = \text{zero}$ , the channel remains closed. In order for the model to fit the published experimental data, each O-domain must be cooperative ( $n = 2$ ) and have lower affinity and faster  $\text{Ca}^{2+}$ -binding kinetics than each A-domain (Fig. 1, methods). At high  $[\text{Ca}^{2+}]$ , when both O- and A-domains are occupied, the data are best fit if the channel opens 75% of the time when  $O = A$ .

This model predicts that the steady-state probability of a channel being open ( $P_o$ ) varies as a monotonic increasing function of  $[\text{Ca}^{2+}]$  (Fig. 1A) and that fast  $\text{Ca}^{2+}$  steps trigger transient bursts of channel activity well above the steady-state level (Fig. 1, A and B). The predicted concentration- and time-dependent occupancy of O- and A-domains on a tetramer during two step increases in  $[\text{Ca}^{2+}]$  are

shown (Fig. 1C). Our model accurately accounts for the experimental data which defines RyR adaptation (1). Published models (3) cannot reproduce the observed second transient response of the "apparently inactivated" channel. This is expected in light of theoretical thermodynamic analysis of RyR behavior, which indicates that one would need a large number of  $\text{Ca}^{2+}$ -binding sites to explain adaptation (4).

Our adaptation model resolves apparently contradictory results and suggests future areas of experimentation. The model explains how elevated  $[\text{Ca}^{2+}]$  can both apparently "inactivate" peak SR  $\text{Ca}^{2+}$  release in situ and increases steady-state  $P_o$  of individual RyR channels. It also enables the SR  $\text{Ca}^{2+}$  release channels to respond to  $d[\text{Ca}^{2+}]/dt$ , a classical observation of Fabiato (3) in skinned muscle. Adaptation in vitro, however, appears too slow to regulate SR  $\text{Ca}^{2+}$  release in cells (1, 5). Thus, the model predicts that (as yet) unknown endogenous factors may accelerate the rate of adaptation (for example, modulate binding kinetics of A-domain) in cells. Finally, this model may apply to other intracellular  $\text{Ca}^{2+}$  release channels as it could also provide the basis for the incremental, or "quantal,"  $\text{Ca}^{2+}$  release from inositol triphosphate ( $\text{IP}_3$ )-sensitive  $\text{Ca}^{2+}$  stores (6). [An  $\text{IP}_3$  receptor channel tetramer with O- and A-domains incrementally occupied by  $\text{IP}_3$  may explain the quantal character of the  $\text{IP}_3$ -induced channel opening as well as the incremental channel "inactivation" observed by Hajnoczky and Thomas (6)].

Thus, we propose that the complex adaptive channel behavior arises from the assembly of simple interactive monomers. Although each monomer by itself is not able to produce the complex behavior, the interplay among the monomers exponentially extends the functional flexibility of the assembled unit.